AIAA JOURNAL
Vol. 43, No. 3, March 2005

Effect of Numerics on Navier–Stokes Computations of Hypersonic Double-Cone Flows

Marie-Claude Druguet*
Université de Provence, 13453 Marseille Cedex 13, France
and
Graham V. Candler† and Ioannis Nompelis‡
University of Minnesota, Minneapolis, Minnesota 55455

A systematic study of the effects of the numerics on the simulation of a steady hypersonic flow past a sharp double cone is presented. Previous studies have shown that the double-cone flow is challenging to compute, making it useful for testing both numerical schemes and physical models. We focus on the numerical aspects only and show that the results are very sensitive to the numerical flux evaluation method and slope limiter used. We find that, when the grid is fine enough, all of the flux evaluation schemes give the same results, though this may require a very large number of points for the most dissipative schemes. The least dissipative schemes have the great advantage of giving accurate results on a coarser grid and are, therefore, less costly. Interestingly, it is also shown that the modified Steger–Warming solver gives as accurate results as other well-known high-quality schemes, such as the Roe scheme with the van Leer slope limiter. Finally, note that an efficient approach such as a parallel implicit method was required.

I. Introduction

THE hypersonic flow over a double-cone geometry is an interesting computational fluid dynamics (CFD) case because it produces many of the complex phenomena, such as shock interactions, triple points, and recirculation zones, that take place in flows past hypersonic vehicles. These vehicles will likely have regions of separated flow, for example, near control surfaces and behind flame holders. Additionally, shock–shock interactions and shocks impinging on the vehicle surface cause high localized aerothermal loads. Figure 1 shows a schematic of a double-cone flowfield. The attached leading-edge shock wave interacts with a detached bow shock wave formed from the second cone, and this interaction produces a transmitted shock wave that impinges on the second cone surface. This produces very high surface pressures and heat transfer rates on the second cone. Because of the high pressures at the impingement location, the flow separates near the cone–cone juncture and a recirculation zone develops, which in turn alters the shock interaction. The size of the separation zone is very sensitive to the shock angles and to the strength of the shock interaction. Downstream of the shock impingement location, a supersonic jet develops near the second cone surface.

The double-cone flow simulated in the present work was designed as a CFD validation test case with fully laminar flow and minimal effects of vibrational relaxation and chemical reactions.[1] In a separate study, we have made a careful examination of the double-cone flow to understand discrepancies between experimental data and simulations.[2] In that work, we found that the vibrational nonequilibrium in the tunnel freestream and weak accommodation of vibrational energy to the surface were responsible for the observed differences.

In the present paper, we focus on the numerical issues associated with simulating the double-cone flow and neglect the physical modeling aspects of the problem. Therefore, we are not attempting to reproduce experimental measurements, but rather to use the double-cone flow as a test case for understanding the properties of a variety of popular numerical schemes. We show that the prediction of the shock interaction and the separation zone are very sensitive to the level of numerical dissipation, which depends on the accuracy of the numerical schemes and on the grid resolution. We compare results obtained with the different schemes to determine how the choice of the flux evaluation method and slope limiter affect the solution quality. We also use several levels of grid refinement to study how each scheme reaches grid convergence. Because very fine grids are necessary to reach grid convergence, we use an implicit time integration method that permits large computational time steps. Because the size of the separation zone strongly depends on the various interactions, and because it is a variable that is easy to track, it will be used to measure quantitatively the accuracy of the numerical solution.

In the remainder of the paper, we discuss the double-cone test conditions, the computational methods used, the temporal convergence properties of the methods, and then how each scheme performs on the double-cone test case. We show that the double-cone is a valuable test case for assessing the performance of CFD methods.

II. Double-Cone Flow Conditions

The flow conditions were obtained from the 25–55-deg double-cone experiments of Holden et al.[3] and Harvey et al.[4] We study run 35, with freestream conditions $T_\infty = 138.9$ K, $\rho_\infty = 5.515 \times 10^{-4}$ kg/m^3, and $u_\infty = 2713$ m/s; the wall temperature is fixed at 296.1 K. These conditions correspond to a Mach number of 11.30 and a unit Reynolds number of 1.333×10^5 m^{-1}. The double-cone geometry has two conical sections of 10.16-cm surface length. For this model scale and these freestream conditions, the flow reaches a steady state during the test time, and the flow is completely laminar. This is supported by analysis of the shear layer Reynolds numbers, the number of characteristic flow times, and the excellent agreement obtained with laminar calculations.[2,4,5]

Presented as Paper 2003-3548 at the AIAA 16th Computational Fluid Dynamics Conference, Orlando, FL, 23–26 June 2003; received 5 November 2003; revision received 9 September 2004; accepted for publication 8 October 2004.

*Chargée de Recherche, Centre National de la Recherche Scientifique Unité Mixte de Recherche 6595, 5, Rue Enrico Fermi; druguet@polytech.univ-mrs.fr. Member AIAA.

†Professor, Department Aerospace Engineering and Mechanics and Army High Performance Computing Research Center, 110 Union Street Southeast; candler@aem.umn.edu. Associate Fellow AIAA.

‡Graduate Research Assistant, Department of Aerospace Engineering and Mechanics and Army High Performance Computing Research Center, 110 Union Street Southeast. Student Member AIAA.

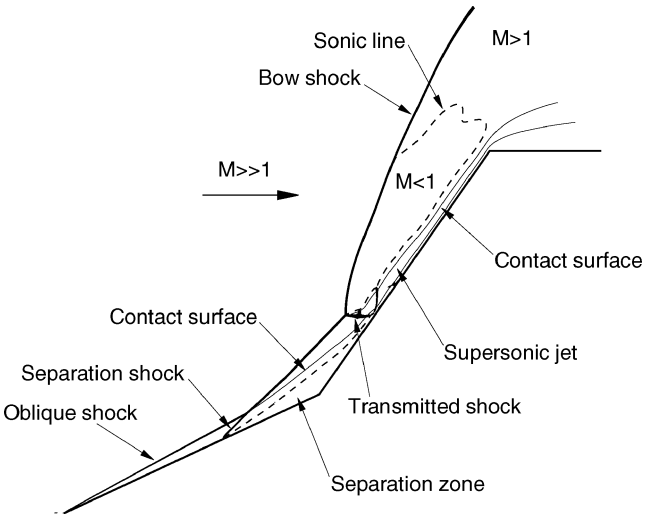

Fig. 1 Schematic of the hypersonic flow past a double-cone geometry.

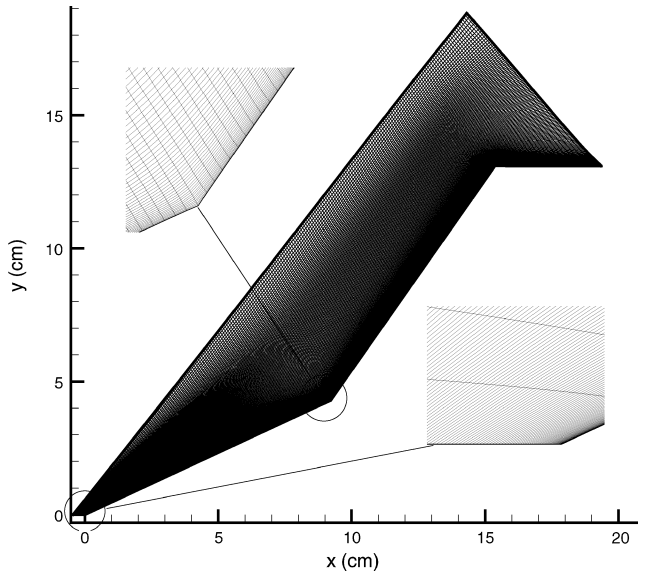

Fig. 2 Grid 256×128 used in study, insets showing expanded views of the tip and cone junction regions.

For this flow, the boundary conditions are supersonic inflow, symmetry on the cone axis, and a no-slip isothermal surface on the cone. The grid is designed so that the flow is either supersonic or in the boundary layer at the outflow (Figs. 1 and 2). Thus, we use a simple zero-gradient extrapolation for the outflow boundary condition; we have verified that there is no upstream influence from this boundary.

As discussed earlier, there are effects of vibrational energy relaxation in the test flow. However, for the purposes of the present numerical study, we neglect these effects and simulate a nonreacting and nonvibrationally excited perfect gas. A complete analysis of the vibrational energy relaxation effects is given in Ref. 2.

III. Computational Procedure

The axisymmetric flow past the sharp double-cone is governed by the compressible, time-dependent Navier–Stokes equations

$$\int_{\mathcal{V}} \frac{\partial \boldsymbol{U}}{\partial t}\,\mathrm{d}\mathcal{V} + \int_{\mathcal{S}} \boldsymbol{F}\cdot n\,\mathrm{d}\mathcal{S} = \int_{\mathcal{V}} \boldsymbol{W}\,\mathrm{d}\mathcal{V} \tag{1}$$

where $\boldsymbol{U} = (\rho, \rho u, \rho v, \rho e)'$ is the vector of conserved variables, $\boldsymbol{F}$ the vector of convective and dissipative fluxes, and $\boldsymbol{W}$ the vector of axisymmetric source terms. Because the gas is nonreactive, the transport coefficients are computed according to the usual laws: The fluid viscosity is temperature dependent and is given by Sutherland's law, $\mu = 1.458\times10^{-6}\,T^{3/2}/(T+110.4)$ kg/m s; the thermal conductivity is given by $\lambda = \mu c_p/Pr$, where c_p is the specific heat at constant pressure; and the Prandtl number $Pr = 0.72$.

The equations are discretized in space according to the finite volume method, where the fluxes at the interfaces of each cell are evaluated with approximate Riemann solvers. These include the Roe scheme with the entropy fix H-correction,[6] the Lax–Friedrichs (LF), the Harten–Lax–van Leer (HLL) and the Harten–Lax–van Leer contact[7] (HLLC) schemes, plus the modified Steger–Warming solver. To ensure high-order accuracy of the flux evaluation, the conservative variables are reconstructed at the cell interfaces by means of second-order accurate reconstruction schemes. To prevent oscillations in these high-order reconstruction schemes, the slopes must be limited. A choice of limiters for this study includes minmod, van Albada, van Leer, and superbee (see Ref. 7). The different schemes used in our study are well documented in the literature, except for the modified Steger–Warming approach, which is presented here. We will see that this scheme is as attractive as more sophisticated schemes such as the Roe scheme.

Recently, Gaitonde et al.[5] conducted a careful time convergence study on this test case and showed that the solution does not converge until at least 100 characteristic flow times have been computed. This relatively long timescale allows the separation zone to become fully established. They define the characteristic time to be the time required to travel the length ℓ of the double-cone model at the freestream velocity, $\tau_{\text{char}} = \ell/u_\infty$. Our computations are consistent with their findings, and we simulate our flows to a minimum of 150 flow times.

To obtain the grid-converged solution, we use grids where the smallest dimension $\Delta y_{\min}$ is of the order of 0.1 μm. For stability reasons, the explicit computational time allowed, in which the Courant–Friedrichs–Lewy (CFL) number plays a role, is $\tau_{\text{expl}} \simeq \text{CFL}_{\text{expl}} \times \Delta y_{\min}/u_\infty$, where CFL_{expl} must be smaller than unity. Then, to obtain the steady-state solution with an explicit time integration method, we would need N_{expl} iterations, with $N_{\text{expl}} = 100\,\tau_{\text{char}}/\tau_{\text{expl}}$. With the characteristic size ℓ being about 0.2 m, N_{expl} is at least 2×10^8. It would be impossible to run an explicit Navier–Stokes code for this huge number of time steps, and we must use an approach that converges more rapidly than an explicit method. In the present work, we use an implicit time integration approach; however, multigrid or Newton–Krylov methods could potentially be used to accelerate convergence.

With implicit time integration, it is well known that the time accuracy may be lost because the time step is chosen to be as large as possible and because the number of sweeps of the relaxation procedure within each iteration is not large enough to ensure a complete convergence of the nonlinear update. Therefore, although we monitor the number of characteristic flow times as a measure of convergence to steady-state, we also use the residual and separation zone size to determine when the solution is converged.

A. Modified Steger–Warming Flux Vector Splitting

The original Steger–Warming flux vector splitting method[8] uses the fact that the inviscid flux vector $\boldsymbol{F}$ is homogeneous in the vector of conserved variables $\boldsymbol{U}$. Thus, we can write

$$\boldsymbol{F} = \frac{\partial \boldsymbol{F}}{\partial \boldsymbol{U}}\boldsymbol{U} = A\boldsymbol{U}$$

Now, if we diagonalize the Jacobian A such that

$$A = S^{-1}\Lambda S$$

with S the matrix of the eigenvectors, we can then split the fluxes into forward and backward moving components depending on the sign of the eigenvalues. That is,

$$\boldsymbol{F}_+ = S^{-1}\Lambda_+ S\boldsymbol{U} = A_+\boldsymbol{U} \tag{2}$$

$$\boldsymbol{F}_- = S^{-1}\Lambda_- S\boldsymbol{U} = A_-\boldsymbol{U} \tag{3}$$

where $\Lambda_\pm$ are the diagonal matrices containing the positive and negative values of Λ. Note that $\boldsymbol{F} = \boldsymbol{F}_+ + \boldsymbol{F}_-$.

The Steger–Warming approach has the "sonic glitch" problem[9] when any of the eigenvalues approach zero. Therefore, we use the correction that smoothly limits the eigenvalues according to

$$\tilde{\lambda}_\pm = \tfrac{1}{2}\left(\lambda_\pm \pm \sqrt{\lambda_\pm^2 + \epsilon^2 a^2}\right)$$

where a is the local speed of sound and ϵ is a small value. We find that to prevent the carbuncle phenomenon in the stagnation regions of hypersonic blunt-body flows, we use a value of $\epsilon = 0.3$ with the modified Steger–Warming approach. However, to obtain high-quality boundary-layer solutions, we set $\epsilon = 0$ in the direction normal to solid surfaces.

It is necessary to evaluate the split fluxes at the finite volume surfaces. For a first-order-accurate method, Steger and Warming used a simple upwind approach, which, for the cell face $i + 1/2$ between cell centers i and $i + 1$, is

$$\boldsymbol{F}^{\mathrm{SW}}_{+\,i+\frac{1}{2}} = A_{+\,i}\boldsymbol{U}_i \tag{4}$$

$$\boldsymbol{F}^{\mathrm{SW}}_{-\,i+\frac{1}{2}} = A_{-\,i+1}\boldsymbol{U}_{i+1} \tag{5}$$

where the variables are evaluated at the cell centers denoted by their subscripts. A second-order accurate method is constructed by linear projection of the conserved variable vector to the cell surface. This approach results in large artificial mixing across shear layers that results in excessive dissipation.[10]

We can improve the Steger–Warming approach by simply changing how the split Jacobian matrices are evaluated. In particular, superior performance is obtained if the Jacobians are evaluated with the same data. For example, the following results in a much less dissipative scheme:

$$\boldsymbol{F}^{\mathrm{mod.\,SW}}_{+\,i+\frac{1}{2}} = A_{+\,i+\frac{1}{2}}\boldsymbol{U}_i \tag{6}$$

$$\boldsymbol{F}^{\mathrm{mod.\,SW}}_{-\,i+\frac{1}{2}} = A_{-\,i+\frac{1}{2}}\boldsymbol{U}_{i+1} \tag{7}$$

where $A_{\pm\,i+1/2}$ is evaluated with an appropriate average of the left and right data. We find that calculating a simple average of the primitive variables, rather than the conserved variables, gives the best results.

The preceding method is only first-order accurate, which, of course, is not adequate for most applications. To make it second-order accurate, we can simply project the conserved variables to the surface

$$\boldsymbol{F}^{\mathrm{mod.\,SW}}_{+\,i+\frac{1}{2}} = A_{+\,i+\frac{1}{2}}\boldsymbol{U}^L_{i+\frac{1}{2}} \tag{8}$$

$$\boldsymbol{F}^{\mathrm{mod.\,SW}}_{-\,i+\frac{1}{2}} = A_{-\,i+\frac{1}{2}}\boldsymbol{U}^R_{i+\frac{1}{2}} \tag{9}$$

with an upwind approach

$$\boldsymbol{U}^L_{i+\frac{1}{2}} = \tfrac{3}{2}\boldsymbol{U}_i - \tfrac{1}{2}\boldsymbol{U}_{i-1} \tag{10}$$

$$\boldsymbol{U}^R_{i+\frac{1}{2}} = \tfrac{3}{2}\boldsymbol{U}_{i+1} - \tfrac{1}{2}\boldsymbol{U}_{i+2} \tag{11}$$

or with the more accurate upwind-biased MUSCL scheme

$$\boldsymbol{U}^L_{i+\frac{1}{2}} = \boldsymbol{U}_i + \tfrac{1}{6}(\boldsymbol{U}_i - \boldsymbol{U}_{i-1}) + \tfrac{1}{3}(\boldsymbol{U}_{i+1} - \boldsymbol{U}_i) \tag{12}$$

$$\boldsymbol{U}^R_{i+\frac{1}{2}} = \boldsymbol{U}_{i+1} - \tfrac{1}{3}(\boldsymbol{U}_{i+1} - \boldsymbol{U}_i) - \tfrac{1}{6}(\boldsymbol{U}_{i+2} - \boldsymbol{U}_{i+1}) \tag{13}$$

The latter projection is more accurate, and we have used it for the simulations presented here.

This method must be limited to prevent oscillations near discontinuities. We can use a standard slope limiter on the projection to make the scheme total variation diminishing, or we can use a simpler pressure-based limiter that makes the scheme revert to the first-order fluxes when $|p_{i+1} - p_i| > \sigma_1 \min(p_{i+1}, p_i)$, where we set $\sigma_1 = 0.75$.

This approach works well for most flows, but in the vicinity of strong shock waves, oscillations can develop. To eliminate this problem, we cause the Jacobian evaluation to revert smoothly to the original Steger–Warming approach in regions of large pressure gradient. One approach is to compute the normalized pressure gradient, $\nabla\tilde{p} = \sigma_2(p_{i+1} - p_i)/\min(p_{i+1}, p_i)$, and weight the average by the use of this function. For example, one of the velocity components u that is used to evaluate A_+ becomes

$$\bar{u} = (1 - \omega)\,u_i + \omega\,u_{i+1} \tag{14}$$

$$\omega = \tfrac{1}{2}[1/(\nabla\tilde{p}^2 + 1)] \tag{15}$$

and similarly for A_-. Note then that $\bar{u} = (1/2)(u_i + u_{i+1})$ for weak pressure gradients and that $\bar{u} = u_i$ for very strong pressure gradients, which causes the scheme to revert to the original Steger–Warming formulation. We use a value of $\sigma_2 = 0.5$.

The results presented in this paper show that this modification to the Steger–Warming flux vector splitting method is competitive with the best low-dissipation modern schemes. In all cases, we have kept the tunable coefficients ϵ, σ_1, and σ_2 fixed at the values given in the text; experience shows that these values are appropriate for a wide range of hypersonic flows. The modified Steger–Warming approach also has the advantage that the linearization of the fluxes is straightforward, making the development of implicit methods relatively easy.

B. Linearization of the Convective Fluxes

To get an efficient implicit code, it is necessary to linearize the convective and dissipative fluxes and the source terms correctly. The linearization of the dissipative fluxes is available in the literature.[11,12] Here, we derive the expression for the linearized Roe and HLL fluxes.

Globally, the linearization of the fluxes $\boldsymbol{F}$ with respect to time is written as follows:

$$\boldsymbol{F}(\boldsymbol{U}^{n+1}) = \boldsymbol{F}(\boldsymbol{U}^n) + \frac{\partial \boldsymbol{F}}{\partial \boldsymbol{U}}(\boldsymbol{U}^{n+1} - \boldsymbol{U}^n) + \mathcal{O}[(\boldsymbol{U}^{n+1} - \boldsymbol{U}^n)^2] \tag{16}$$

that is written more simply as

$$\boldsymbol{F}^{n+1} = \boldsymbol{F}^n + \frac{\partial \boldsymbol{F}}{\partial \boldsymbol{U}}\delta\boldsymbol{U}^n \tag{17}$$

with $\delta\boldsymbol{U}^n = \boldsymbol{U}^{n+1} - \boldsymbol{U}^n$.

The Roe flux evaluation at the interface $i + 1/2$ between cell centers i and $i + 1$ is written as

$$\boldsymbol{F}^{\mathrm{Roe}^n}_{i+\frac{1}{2}} = \tfrac{1}{2}\left[\boldsymbol{F}(\boldsymbol{U}_i) + \boldsymbol{F}(\boldsymbol{U}_{i+1}) - \left|A^{\mathrm{Roe}}\left(\boldsymbol{U}_{M_{i+\frac{1}{2}}}\right)\right|(\boldsymbol{U}_{i+1} - \boldsymbol{U}_i)\right]^n \tag{18}$$

where $\boldsymbol{U}_{M_{i+1/2}}$ is an average of $\boldsymbol{U}_i$ and $\boldsymbol{U}_{i+1}$ and where the Roe dissipative matrix A^{Roe} can be diagonalized as

$$|A^{\mathrm{Roe}}| = S^{-1}|\Lambda|S \tag{19}$$

with Λ the diagonal matrix of the Roe eigenvalues and S^{-1} and S the matrices of the right and left eigenvectors. For writing convenience, we set $|A^{\mathrm{Roe}}|(\boldsymbol{U}^n_{i+1} - \boldsymbol{U}^n_i) = \boldsymbol{H}^n_{i+1/2}$ and $\boldsymbol{F}(\boldsymbol{U}^n_i) = \boldsymbol{F}^n_i$.

Each term of the Roe fluxes must be written at the time $n + 1$ and linearized as follows:

$$\boldsymbol{F}^{n+1}_i = \boldsymbol{F}^n_i + A^{L^n}_{i+\frac{1}{2}}\delta\boldsymbol{U}^n_i \tag{20}$$

$$\boldsymbol{F}^{n+1}_{i+1} = \boldsymbol{F}^n_{i+1} + A^{R^n}_{i+\frac{1}{2}}\delta\boldsymbol{U}^n_{i+1} \tag{21}$$

$$\boldsymbol{H}^{n+1}_{i+\frac{1}{2}} = \boldsymbol{H}^n_{i+\frac{1}{2}} + \left|A^{\mathrm{Roe}^n}_{i+\frac{1}{2}}\right|\left(\delta\boldsymbol{U}^n_{i+1} - \delta\boldsymbol{U}^n_i\right) \tag{22}$$

where $A^{L^n}_{i+1/2} = \partial \boldsymbol{F}^n_i / \partial \boldsymbol{U}^n_i$ and $A^{R^n}_{i+1/2} = \partial \boldsymbol{F}^n_{i+1} / \partial \boldsymbol{U}^n_{i+1}$, and where it is assumed that $|A^{\mathrm{Roe}^n}_{i+1/2}|$ is frozen during the linearization of $\boldsymbol{H}^n_{i+1/2}$. There is no special work to do to derive $A^{L^n}_{i+1/2}$ and $A^{R^n}_{i+1/2}$: They have the same expression as $|A^{\mathrm{Roe}^n}_{i+1/2}|$ where we replace $\boldsymbol{U}_{M_{i+1/2}}$ by $\boldsymbol{U}_i$ and $\boldsymbol{U}_{i+1}$, respectively. Then the linearized Roe flux reads

$$\boldsymbol{F}^{\mathrm{Roe}^{n+1}}_{i+\frac{1}{2}} = \boldsymbol{F}^{\mathrm{Roe}^n}_{i+\frac{1}{2}} + \tfrac{1}{2}\left(A^{L^n}_{i+\frac{1}{2}} + \left|A^{\mathrm{Roe}^n}_{i+\frac{1}{2}}\right|\right)\delta \boldsymbol{U}^n_i + \tfrac{1}{2}\left(A^{R^n}_{i+\frac{1}{2}} - \left|A^{\mathrm{Roe}^n}_{i+\frac{1}{2}}\right|\right)\delta \boldsymbol{U}^n_{i+1} \tag{23}$$

$$= \boldsymbol{F}^{\mathrm{Roe}^n}_{i+\frac{1}{2}} + A^{-n}_{i+\frac{1}{2}}\delta \boldsymbol{U}^n_i + A^{+n}_{i+\frac{1}{2}}\delta \boldsymbol{U}^n_{i+1} \tag{24}$$

Because the LF scheme has the same form as the Roe scheme, the linearization of its fluxes follows the same procedure.

The HLL flux evaluation is written as

$$\boldsymbol{F}^{\mathrm{HLL}^n}_{i+\frac{1}{2}} = \begin{cases} \boldsymbol{F}^n_i & \text{if} \quad 0 \le s^L_{i+\frac{1}{2}} \\ \dfrac{s^R_{i+\frac{1}{2}}\boldsymbol{F}^n_i - s^L_{i+\frac{1}{2}}\boldsymbol{F}^n_{i+1} + s^L_{i+\frac{1}{2}}s^R_{i+\frac{1}{2}}\left(\boldsymbol{U}^n_{i+1} - \boldsymbol{U}^n_i\right)}{s^R_{i+\frac{1}{2}} - s^L_{i+\frac{1}{2}}} & \text{if} \quad s^L_{i+\frac{1}{2}} \le 0 \le s^R_{i+\frac{1}{2}} \\ \boldsymbol{F}^n_{i+1} & \text{if} \quad 0 \ge s^R_{i+\frac{1}{2}} \end{cases} \tag{25}$$

with the slopes $s^R_{i+1/2} = s_{i+1}$ and $s^L_{i+1/2} = s_i$ defined by the HLL scheme (see Ref. 7). It is linearized as follows:

$$\frac{\partial \boldsymbol{F}^{\mathrm{HLL}^n}_{i+\frac{1}{2}}}{\partial \boldsymbol{U}_i} = A^{-n}_{i+\frac{1}{2}} = \begin{cases} A^{L^n}_{i+\frac{1}{2}} & \text{if} \quad 0 \le s^L_{i+\frac{1}{2}} \\ \dfrac{s^R_{i+\frac{1}{2}}\left(A^{L^n}_{i+\frac{1}{2}} - s^L_{i+\frac{1}{2}}I\right)}{s^R_{i+\frac{1}{2}} - s^L_{i+\frac{1}{2}}} & \text{if} \quad s^L_{i+\frac{1}{2}} \le 0 \le s^R_{i+\frac{1}{2}} \\ 0 & \text{if} \quad 0 \ge s^R_{i+\frac{1}{2}} \end{cases} \tag{26}$$

$$\frac{\partial \boldsymbol{F}^{\mathrm{HLL}^n}_{i+\frac{1}{2}}}{\partial \boldsymbol{U}_{i+1}} = A^{+n}_{i+\frac{1}{2}} = \begin{cases} 0 & \text{if} \quad 0 \le s^L_{i+\frac{1}{2}} \\ \dfrac{s^L_{i+\frac{1}{2}}\left(s^R_{i+\frac{1}{2}}I - A^{R^n}_{i+\frac{1}{2}}\right)}{s^R_{i+\frac{1}{2}} - s^L_{i+\frac{1}{2}}} & \text{if} \quad s^L_{i+\frac{1}{2}} \le 0 \le s^R_{i+\frac{1}{2}} \\ A^{R^n}_{i+\frac{1}{2}} & \text{if} \quad 0 \ge s^R_{i+\frac{1}{2}} \end{cases} \tag{27}$$

Then the linearized HLL flux reads

$$\boldsymbol{F}^{\mathrm{HLL}^{n+1}}_{i+\frac{1}{2}} = \boldsymbol{F}^{\mathrm{HLL}^n}_{i+\frac{1}{2}} + A^{-n}_{i+\frac{1}{2}}\delta \boldsymbol{U}^n_i + A^{+n}_{i+\frac{1}{2}}\delta \boldsymbol{U}^n_{i+1} \tag{28}$$

that has the same general form as Eq. (24).

The HLLC scheme (see Ref. 7), which corrects the HLL scheme by restoring the missing contact wave is constructed in a similar fashion. Therefore, we use the linearization of the HLL fluxes for the HLLC fluxes as well. The code runs with no problem with such an approximation, and similar time steps have been used for both methods, though the HLLC convergence rate is degraded somewhat.

The preceding linearization is done for the fluxes across the four cell interfaces: $\boldsymbol{F}_{i+1/2,j}$, $\boldsymbol{F}_{i-1/2,j}$, $\boldsymbol{G}_{i,j+1/2}$, and $\boldsymbol{G}_{i,j-1/2}$. The source terms of the conservation equation are also linearized:

$$\boldsymbol{W}^{n+1}_i = \boldsymbol{W}^n_i + C^n_i \delta \boldsymbol{U}^n_i \tag{29}$$

where $C^n_i = \partial \boldsymbol{W}^n_i / \partial \boldsymbol{U}^n_i$. The time integration is implicit and performed with the data parallel line relaxation (DPLR) method,[13] where the time step is global on the computational domain.

IV. Grid Design

The double-cone flow has several critical flow features that require careful grid generation. First, at the tip of the first cone, the grid must be well resolved to capture the boundary layer that starts developing at this location. At the junction of the two cones, the grid lines must be smooth to not introduce artificial perturbation. There is also a tradeoff between resolving the boundary layer and the shock interaction triple point. Figure 2 shows the coarse 256×128 grid with expanded views of the critical tip and cone juncture regions. Note that the grid is highly stretched to the surface and that care has been taken to maintain grid regularity and smoothness as much as possible. We have used up to five levels of grid refinement: 256×128 (coarse), 512×256 (medium), 1024×512 (fine), 1536×768 (very fine), and 2048×1024 (ultrafine). For all grid levels, we have generated a grid that balances the preceding factors.

V. Time Convergence

The double-cone flowfields are initialized with freestream conditions, and the solution is integrated in time until it reaches a steady state and the residual has decreased by five orders of magnitude. As mentioned earlier we also monitor the total solution time and the separation zone size to verify that the solution has converged.

The use of an implicit method allows us to run at time steps as large as possible to obtain results with the smallest number of iterations and, therefore, within the shortest computational time. Note that the exact linearization of the fluxes makes a significant difference in the convergence properties of the implicit method. In the present study, most computations used time steps of the order of 1/100th–1/1000th of the characteristic flow time. Thus, given that the flowfield requires at least 100 flow times to establish,[5] the solutions should require roughly 10^4–10^5 time steps to reach convergence. However, even if the implicit code can be run with very large time steps, it is not always beneficial to use the largest possible time steps. If the time step is too large, the computation may not converge as quickly as with a smaller time step; the residual may oscillate without decreasing, even if the flow has already attained its steady state. If the time step is even larger, the shock position keeps oscillating, and the flow never reaches a steady state. Thus, there is an optimal value of the maximum time step for each method.

Table 1 presents the number of time steps required for the solution to converge for a variety of methods on two grids. Each method requires essentially the same computational cost per time step, and, thus, the solution cost is proportional to the number of iterations. Note that, in general, the modified Steger–Warming and Roe schemes have the best convergence properties, for example, the Roe scheme requires one-fifth the number of time steps of the HLL scheme on the fine grid. However, when the Roe scheme is used with the less dissipative limiters (van Albada, van Leer, or superbee), it converges poorly. The location where the residual remains high with these slope limiters is in the core of the detached bow shock on the second cone. In this region, the solution at the shock oscillates between slightly different states over a range of time steps. However, these temporal oscillations do not prevent the solution from converging to a unique steady state. We could likely alleviate this problem by shock aligning the grid in this region.

In the double-cone flow, the size of the time step is determined by the minimum near-wall grid spacing, the local speed of sound (at essentially the wall temperature), and the CFL number used for the simulation. The near-surface grid spacing decreases by a factor of 16 between the 256×128 and 1024×512 grids. Therefore, the

Table 1 Approximate number of time steps for each method to converge on the coarse and fine grids

Grid	Modified SW	Roe superbee	Roe van Leer	Roe minmod	LF minmod	HLL minmod	HLLC minmod
256×128	6,000	9,000	6,000	8,000	15,000	19,000	31,000
1024×512	40,000	——	——	60,000	240,000	300,000	400,000

increase in the number of time steps is actually less than expected based on simple CFL number scaling. For example, the Roe plus minmod simulations require 7.5 times as many time steps on the fine grid, rather than the factor of 16 expected. This is because we are able to run the fine-grid simulation with a larger CFL number; in this case, the coarse grid case was run with CFL = 200, whereas the fine grid used CFL = 5000. The LF, HLL, and HLLC simulations were run with maximum CFL numbers of 100 to account for the slower convergence rates.

VI. Results

In this section, we discuss the effect of the numerics on the flows with shock interactions, with emphasis on the effect of the numerical dissipation. The flow about a double cone is well suited for this type of study because the shock interaction and the size of the separation zone strongly depend on the global features of the flow. For example, a slight change in the angle of the oblique shock wave attached to the first cone makes the interaction with the bow shock wave different, changing the size of the separation zone. We first show the global behavior of the flow, then the surface quantities, and finally the size of the separation zone. Because the size of the recirculation zone is very sensitive to changes in the general flow features, and because it is a simple variable to track, it is used for quantitative comparisons.

To show the influence of the numerical dissipation on these flows, a range of more or less dissipative flux evaluation schemes has been used. That includes a set of flux evaluation schemes, modified Steger–Warming, LF, HLL, HLLC, and Roe, and a set of slope limiters, minmod, van Albada, van Leer, and superbee. We know beforehand the dissipation characteristics of each scheme. The LF scheme is known to be extremely dissipative. The HLL scheme is known for its inability to capture contact surfaces because its construction relies only on the acoustic waves. The HLLC scheme is more reliable because it was built to remedy the weaknesses of the HLL scheme. The Roe scheme is known to be accurate with good dissipation properties. The classical Steger–Warming (SW) scheme is known to be dissipative, but we will see that this is not true for the modified SW. With regard to the slope limiters, minmod is known to be dissipative, whereas superbee can introduce undesired oscillations. We will see in the following results how all of these schemes and slope limiters behave for the simulation of the double-cone flow.

A. Coarse Grid Results

First, we present results obtained on the coarse 256×128 grid to demonstrate the effects of the numerics when the flow is underresolved. In Fig. 3, we show the shock location computed with different solvers (modified SW, LF, Roe, HLL, and HLLC). For those computations, all of the flux evaluation schemes except the modified SW use the minmod slope limiter. It is easily seen that the location of the separation shock and the size of the recirculation zone vary with the schemes. The results show that the least dissipative schemes (modified SW, Roe, and HLLC) give the largest recirculation zone. The most dissipative schemes (LF and HLL) artificially increase the mixing in the separation zone, thereby reducing its size. Thus, the effect of numerical dissipation is similar to an increase in the viscous dissipation, resulting in a smaller effective Reynolds number. This is consistent with the lowering of the Reynolds number in a laminar flow reducing the separation zone size.[3]

The modified SW method gives the largest recirculation zone because this scheme uses a good reconstruction scheme that is not as dissipative as the other methods because of the dissipative minmod slope limiter. Figure 4 shows that if the Roe scheme is used with a less dissipative slope limiter, its results are significantly better and

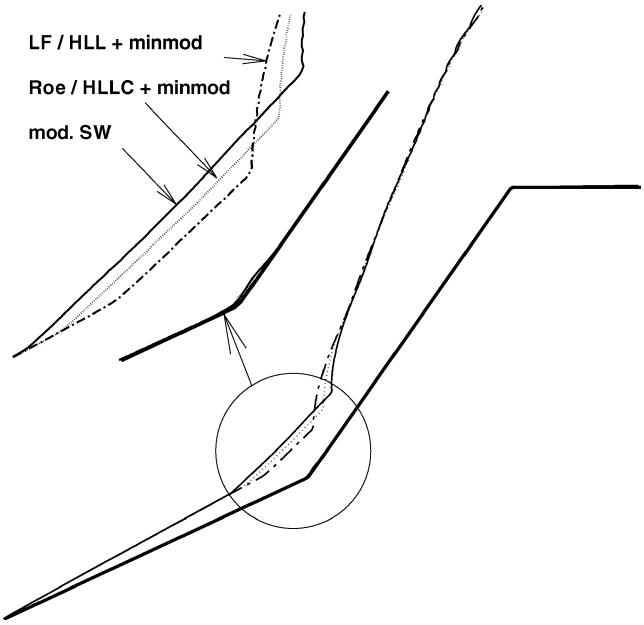

Fig. 3 Bow shock location ($T = 400$ K contour) computed with different solvers on 256×128 grid.

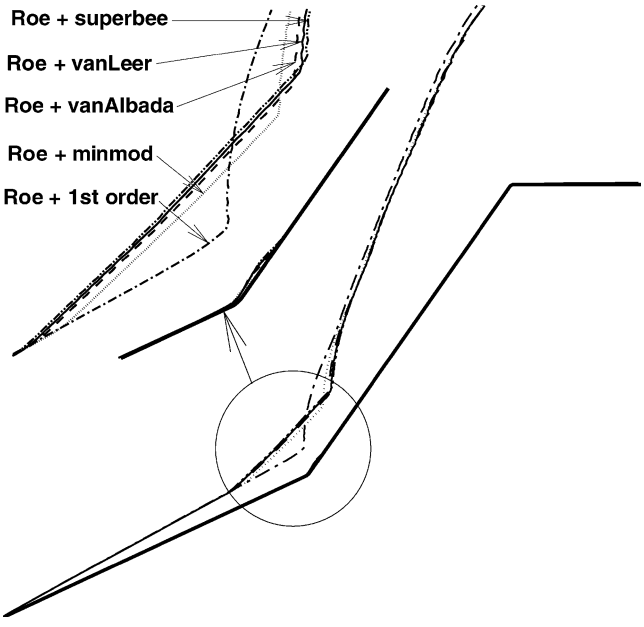

Fig. 4 Bow shock location ($T = 400$ K contour) computed with different slope limiters in association with the Roe scheme on 256×128 grid.

become consistent with the modified SW method. The flowfield computed with Roe plus superbee does not show any spatial oscillations, even though the superbee slope limiter is known to produce oscillations in the simulations of one-dimensional shock waves.[7]

These results are apparent in Figs. 5 and 6, which show the computed and measured surface heat transfer rates. Here we plot the nondimensional heat transfer rate in terms of the Stanton number, defined as $St = q/\rho_\infty u_\infty^3$, where q is the convective heat transfer

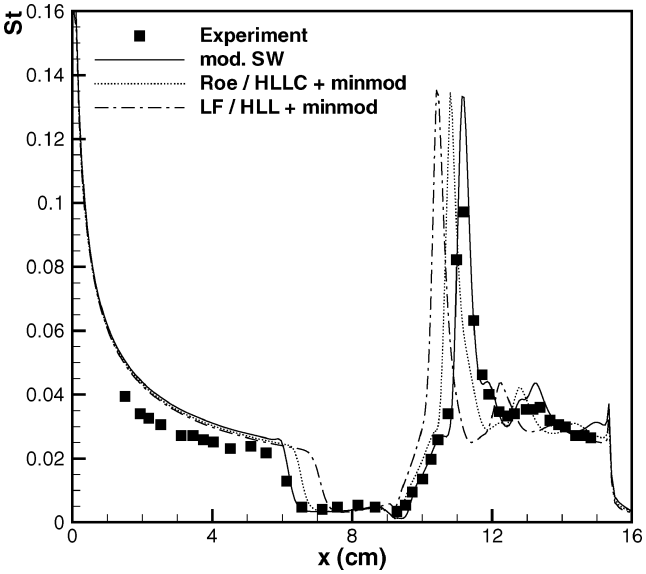

Fig. 5 Heat transfer rate computed with different solvers on 256×128 grid.

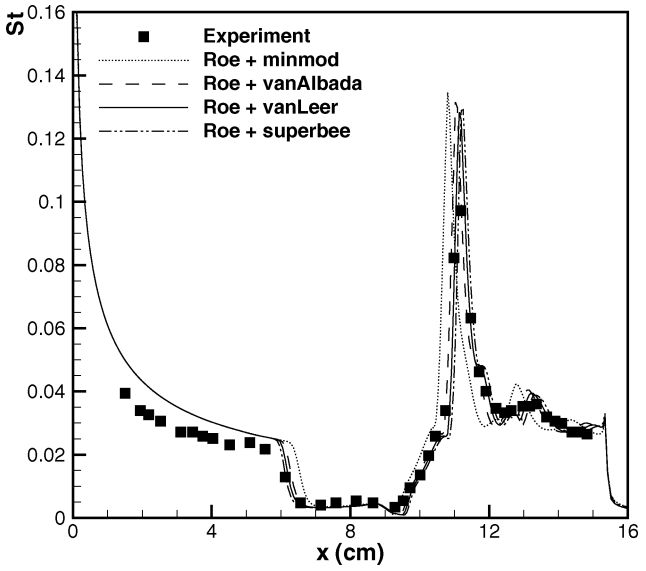

Fig. 6 Heat transfer rate computed with the Roe scheme with different slope limiters on 256×128 grid.

rate to the surface. These results show that, globally, the smaller the separation zone, the larger the heat transfer peak. The size of the separation zone determines where the shock impinges on the surface, which affects the strength of the shock–shock interaction. Again, we see that the size of the separation zone greatly depends on the dissipation of the scheme. For example, the minmod limiter that adds extra dissipation to the Roe scheme results in a smaller separation zone and a larger heat transfer peak than those predicted by the other slope limiters (Fig. 6).

The largest separation zones are given by three solvers: modified SW, Roe plus van Leer, and Roe plus superbee. If we plot the modified SW and Roe plus van Leer results together, we see that they are very similar, and on this grid the modified SW scheme is approximately as accurate as the Roe scheme. If we classify the limiters from the smallest to the largest size of the recirculation zone, we have minmod, van Albada, van Leer, and then superbee. This order corresponds exactly to the classification of the slope limiters according to decreasing dissipation for one-dimensional problems.[7]

Figures 5 and 6 also plot the measured heat transfer rates for the experimental run 35 (Refs. 3 and 4). However, these values are misleading in that the present simulations do not account for critical physical effects, and, thus, the apparent good agreement of the separation zone size achieved with the low-dissipation schemes is spurious. The simulations overpredict the heat transfer rate to the first cone in the attached region because of unmodeled physics in the present work. A complete study that models the effects of vibrational nonequilibrium and incomplete surface accommodation is available in Ref. 2. Therefore, the experimental data points should be used for reference only and not for comparing the accuracy of any given solution.

B. Grid Convergence

The preceding results were obtained on the coarse 256 × 128 grid; now let us consider what happens when we perform a systematic grid convergence study. First consider Fig. 7, which is the heat transfer rate computed with the low-dissipation Roe plus superbee method on a sequence of four grids. There is a significant change in the solution between the coarse grids, but then the solutions appear to be identical to one another. Quantitatively, the separation zone increases by 8.8, 1.7, and 0.2% between the different grids. Also note that, with the grids used in this study, the heat transfer rate for the attached portion of the flow does not vary significantly as the

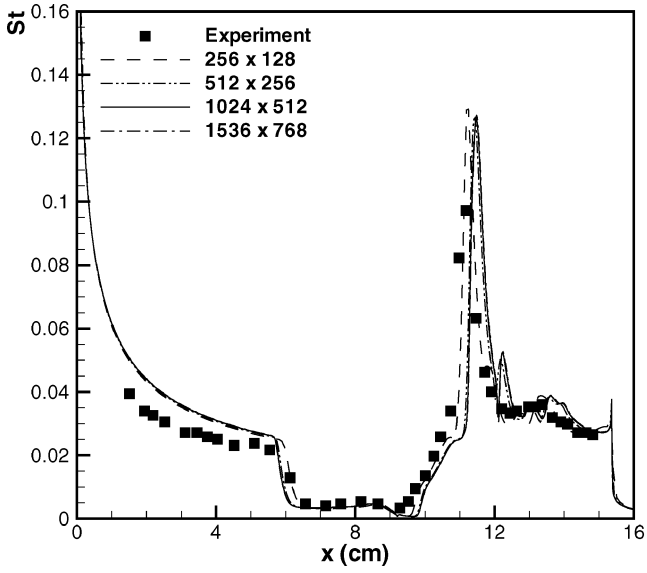

Fig. 7 Heat transfer rate computed on different grids with Roe scheme and superbee slope limiter.

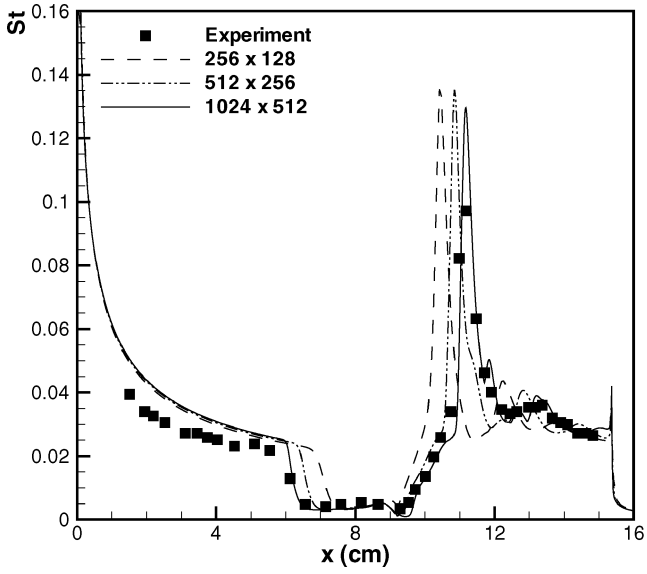

Fig. 8 Heat transfer rate computed on different grids with LF scheme and minmod slope limiter.

Table 2 Size of the separation zone for different grids and schemes

L, cm	256×128	512×256	1024×512	1536×768	2048×1024
Modified SW	4.9010	5.4575	5.5620	5.6077	5.6083
Roe plus minmod	4.2235	4.9964	5.3856	5.5081	
Roe plus van Albada	4.7196	5.3677	5.5729		
Roe plus van Leer	4.9143	5.4355	5.5891	5.6178	
Roe plus superbee	5.0675	5.5140	5.6060	5.6198	
LF plus minmod	3.2946	4.2702	4.9752		
LF plus van Leer			5.5705		
HLLC plus minmod	4.2177	4.9847	5.3807		
HLL plus minmod	3.3450	4.3074	4.9712		

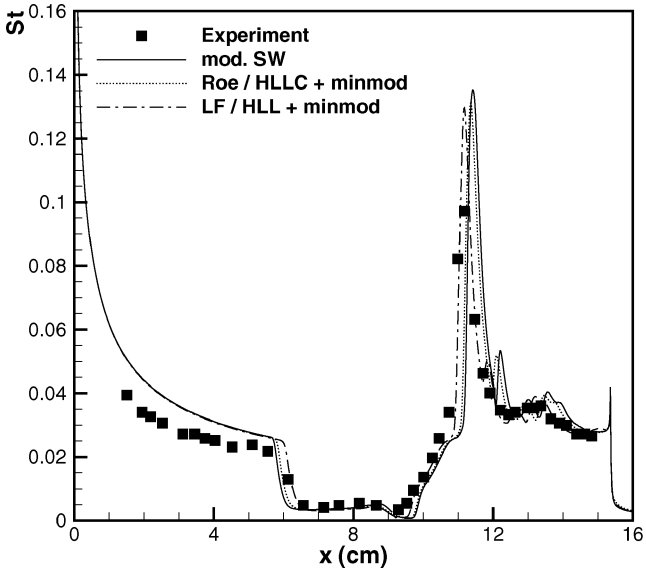

Fig. 9 Heat transfer rate computed with different solvers on 1024×512 grid.

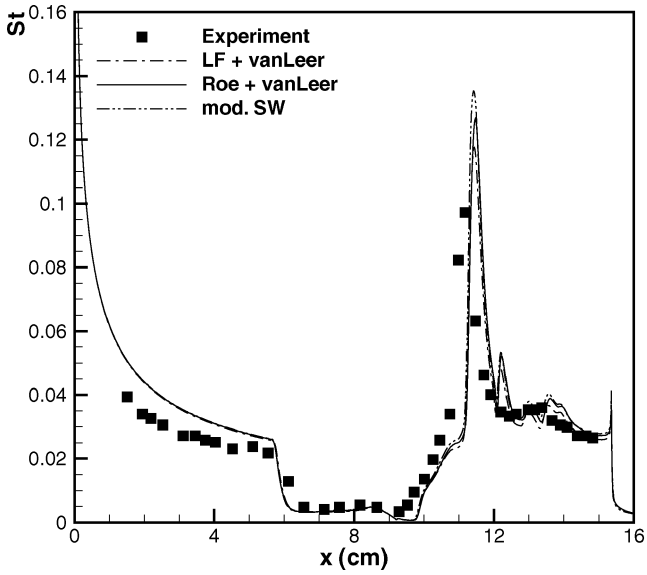

Fig. 10 Heat transfer rate computed with modified SW scheme and Roe and LF schemes with van Leer slope limiter on 1024×512 grid.

grid is refined. This further illustrates that the double-cone flow is most sensitive to the streamwise grid spacing because it determines the resolution of the separation and reattachment points. In any case, we can conclude that the solution systematically converges to a unique solution, and for most purposes, the 512×256 solution with the Roe plus superbee method would be adequate.

Now consider the convergence of the solution with a more dissipative method. Figure 8 is the heat transfer rate computed with the LF plus minmod method for three grids. Note that the solution continues to change, and in comparison to Fig. 7, it is not adequately converged even on the 1024×512 grid. In fact, on this latter grid, the solution is less accurate than Roe plus superbee on the coarse 256×128 grid. This quantitatively illustrates that the hypersonic separated flows must be computed with high-quality, low-dissipation methods.

C. Fine-Grid Results

Now that we have seen that the solvers converge differently, let us compare the results obtained on the fine grid (1024×512). Figure 9 shows the heat transfer rate for the modified SW method and the other solvers with the minmod limiter; again we see that the less dissipative schemes give the largest recirculation zones. In contrast to the results on the coarse grid, the results are now much closer to one another. The most dissipative schemes (LF and HLL) still do not give the same results as the others because they have not yet reached the grid convergence on the 1024×512 grid, as shown in Fig. 8. However, even for the more accurate solvers (Roe or HLLC), the size of the separation zone is still over 3% smaller than that given by the modified SW method. Again, this is because the minmod limiter adds excessive dissipation to the methods. For example, when the LF method is used with the van Leer slope limiter, the separation length increases by 12% on the 1024×512 grid.

Finally, Fig. 10 presents our best results (modified SW and Roe plus van Leer) along with the more dissipative LF plus van Leer method. Note that all methods give very similar results, with the only significant difference being the height of the heat transfer peak at the shock impingement location. We see that the modified SW method gives a slightly larger value than Roe plus van Leer. However, in general, these results agree with one another very well and clearly illustrate the importance of the use of a low-dissipation method for this flow.

D. Evolution of the Size of the Recirculation Zone

For a more quantitative assessment of the methods, consider the size of the separation zone L for each method. We define L as the axial (x) distance between the separation point on the first cone, where the skin-friction coefficient c_f becomes negative, and the reattachment point on the second cone, where c_f becomes positive again. Table 2 lists the separation length for each grid used.

Let us first focus on the separation length for coarse-grid simulations. Note that the Roe plus superbee, Roe plus van Leer, and modified SW methods give the largest values of L; all other methods give small separation lengths, indicating excessive dissipation. The superbee slope limiter is the least dissipative, but careful attention must be paid when it is used because it may introduce undesired spatial oscillations in the high-order reconstruction scheme.[7] A dissipative limiter such as minmod can significantly degrade the quality of a good scheme. Thus, Table 2 shows that for this complex shock-dominated flow, the choice of the slope limiter is at least as important as the choice of the flux evaluation method. For the double-cone flow the best overall choice of slope limiter is the van Leer.

On the 1536×768 grid, the three best methods are within 0.2% of one another, indicating that the different methods converge to the same unique solution. Interestingly, the two Roe-solver-based methods produce solutions that are essentially identical (0.04% difference), whereas the modified SW method asymptotes to a slightly

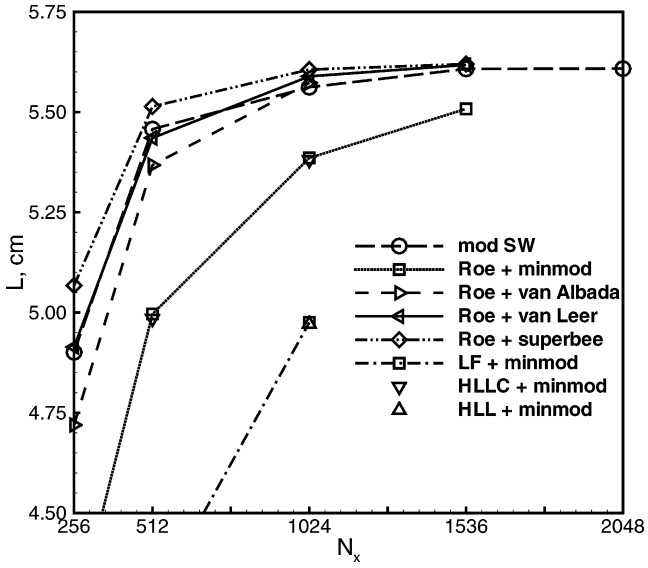

Fig. 11 Size of recirculation zone vs number of grid points in axial (streamwise) direction.

smaller separation length. The reason for this difference is not known; however, note that, on this grid, the axial-direction grid spacing in the vicinity of the separation and reattachment points is 0.01 cm. This is of the same size as the difference between the methods. Therefore, even with this very fine grid, we may not be fully resolving the separation length.

Figure 11 plots L vs N_x, the number of grid points in the streamwise direction of the flow. Figure 11 shows the evolution of the recirculation length as the grid is refined for each method and shows graphically the points made in this paper:

1) The separation length is a good measure of the dissipation qualities of a solution method.

2) All methods converge to the same separation length, though some methods would require an impossibly large number of grid points to achieve convergence.

3) The slope limiter is at least as important as the underlying flux evaluation scheme in these shock-dominated flows.

4) The modified SW, Roe plus superbee, and Roe plus van Leer methods are the best for this problem.

5) The van Leer limiter is the best choice for this flow, whereas minmod is a poor choice because it introduces excessive levels of numerical dissipation.

VII. Conclusions

This study shows that the hypersonic flow past a double-cone geometry is an excellent test case for evaluating the accuracy of numerical methods for the compressible Navier–Stokes equations. The size of the separation region at the cone–cone junction is very sensitive to the level of numerical dissipation in the simulation. Therefore, it is possible to evaluate the accuracy of a new method by performing a single simulation and comparing the separation length to those given in Table 2. This gives a direct measure of the accuracy of the method relative to existing popular methods. (The grids used in this study are available from the authors to facilitate this process.)

The comparison between popular flux evaluation methods and slope limiters produces several important conclusions. First, grid convergence may be obtained for any of the nominally second-order accurate methods tested. However, the more dissipative methods require impossibly large amounts of computer time to obtain convergence. For example, a poor method with a dissipative limiter (LF plus minmod) gives worse results on the 1024×512 grid than a good method (Roe plus superbee) on the 256×128 grid. Thus, the accurate methods are much less costly and actually enable the simulation of this type of complex shock-dominated flow.

Another important conclusion is that the choice of slope limiter is critical for simulating double-cone flows. A dissipative limiter such as minmod can significantly decrease the accuracy of a high-quality method. Poor flux evaluation schemes are even more adversely affected by a dissipative limiter. Our results show that the superbee limiter gives the most accurate results, but that it can have stability and convergence problems. Therefore, the best robust limiter for this type of flow is the van Leer limiter. Interestingly, this study shows that the modified SW scheme gives results that are competitive with other well-known accurate methods, such as the Roe scheme.

Finally, we found that it is mandatory to use an implicit method or some other convergence acceleration approach to simulate these flows. Even with a parallel implementation, it is impractical to obtain solutions to this flow with an explicit method; our calculations were run with time steps corresponding to CFL numbers as high as 5000.

Acknowledgments

This work was sponsored in part by the U.S. Air Force Office of Scientific Research, under Grant FA9550-01-1-0114. The views and conclusions contained herein are those of the authors and should not be interpreted as necessarily representing the official policies or endorsements, either express or implied, of the Air Force Office of Scientific Research or the U.S. Government. This work was also sponsored by the U.S. Army High Performance Computing Research Center under the auspices of the Department of the Army, Army Research Laboratory cooperative agreement DAAD191-01-2-0014, the content of which does not necessarily reflect the position or policy of the government, and no official endorsement should be inferred. A portion of the computer time was provided by the University of Minnesota Supercomputing Institute.

References

[1]Candler, G. V., Nompelis, I., and Holden, M. S., "Computational Analysis of Hypersonic Laminar Viscous–Inviscid Interactions," AIAA Paper 2000-0532, Jan. 2000.

[2]Nompelis, I., Candler, G. V., and Holden, M. S., "Effect of Vibrational Nonequilibrium on Hypersonic Double-Cone Experiments," *AIAA Journal*, Vol. 41, No. 11, 2003, pp. 2162–2169.

[3]Holden, M. S., and Wadhams, T. P., "Code Validation Study of Laminar Shock/Boundary Layer and Shock/Shock Interactions in Hypersonic Flow. Part A: Experimental Measurements," AIAA Paper 2001-1031A, Jan. 2001.

[4]Harvey, J. K., Holden, M. S., and Wadhams, T. P., "Code Validation Study of Laminar Shock/Boundary Layer and Shock/Shock Interactions in Hypersonic Flow. Part B: Comparison with Navier–Stokes and DSMC Solutions," AIAA Paper 2001-1031B, Jan. 2001.

[5]Gaitonde, D. V., Canupp, P. W., and Holden, M. S., "Heat Transfer Predictions in a Laminar Hypersonic Viscous/Inviscid Interaction," *Journal of Thermophysics and Heat Transfer*, Vol. 16, No. 4, 2002, pp. 481–489.

[6]Sanders, R., Morano, E., and Druguet, M.-C., "Multidimensional Dissipation for Upwind Schemes: Stability and Applications to Gas Dynamics," *Journal of Computational Physics*, Vol. 145, No. 2, 1998, pp. 511–537.

[7]Toro, E. F., *Riemann Solvers and Numerical Methods for Fluid Dynamics. A Practical Introduction*, Springer, Berlin, 1997, Chaps. 10, 13, and 14.

[8]Steger, J. L., and Warming, R. F., "Flux Vector Splitting of the Inviscid Gas-Dynamic Equations with Applications to Finite Difference Methods," *Journal of Computational Physics*, Vol. 40, No. 2, 1981, pp. 263–293.

[9]Buning, P. G., and Steger, J. L., "Solution of the Two-Dimensional Euler Equations with Generalized Coordinate Transformations Using Flux Vector Splitting," AIAA Paper 82-0971, June 1982.

[10]MacCormack, R. W., and Candler, G. V., "The Solution of the Navier–Stokes Equations Using Gauss–Seidel Line Relaxation," *Computers and Fluids*, Vol. 17, No. 1, 1989, pp. 135–150.

[11]Gnoffo, P. A., "An Upwind-Biased Point Implicit Relaxation Algorithm for Viscous, Compressible Perfect-Gas Flows," NASA TP 2953, Feb. 1990.

[12]Tysinger, T. L., and Caughey, D. A., "Alternating Direction Implicit Methods for the Navier–Stokes Equations," *AIAA Journal*, Vol. 30, No. 8, 1992, pp. 2158–2161.

[13]Wright, M. J., Bose, D., and Candler, G. V., "Data-Parallel Line Relaxation Method for the Navier–Stokes Equations," *AIAA Journal*, Vol. 36, No. 9, 1998, pp. 1603–1609.

J. Bellan
Associate Editor